JACS
JOURNAL OF THE AMERICAN CHEMICAL SOCIETY
Article
pubs.acs.org/JACS

Self-Assembled Chiral Nanofibers from Ultrathin Low-Dimensional Nanomaterials

Chaoliang Tan,[†] Xiaoying Qi,[†] Zhengdong Liu,[†,‡] Fei Zhao,[†,‡] Hai Li,[†,§] Xiao Huang,[†,§] Lin Shi,[∥] Bing Zheng,[†,§] Xiao Zhang,[†] Linghai Xie,[‡] Zhiyong Tang,[∥] Wei Huang,[‡,§] and Hua Zhang*[,†]

[†]School of Materials Science and Engineering, Nanyang Technological University, 50 Nanyang Avenue, Singapore 639798, Singapore

[‡]Key Laboratory for Organic Electronics and Information Displays (KLOEID) and Institute of Advanced Materials (IAM), Jiangsu National Synergetic Innovation Center for Advanced Materials (SICAM), Nanjing University of Posts and Telecommunications, 9 Wenyuan Road, Nanjing 210046, China

[§]Key Laboratory of Flexible Electronics (KLOFE) and Institute of Advanced Materials (IAM), Jiangsu National Synergistic Innovation Center for Advanced Materials (SICAM), Nanjing Tech University (NanjingTech), 30 South Puzhu Road, Nanjing 211816, China

[∥]Laboratory for Nanomaterials, National Center for Nanoscience and Technology, Beijing 100190, P. R. China

Supporting Information

ABSTRACT: Despite many developed methods, it still remains a challenge to provide a simple and general strategy for the controlled preparation of chiral nanostructures. Here we report a facile and universal approach for the high-yield and scalable preparation of chiral nanofibers based on the self-assembly of various ultrathin one-dimensional and two-dimensional nanomaterials in vigorously stirred polymeric solutions. The obtained chiral nanofibers can be further transformed to same-handed chiral nanorings. As a proof-of-concept application, chiral MoS_2 and multiwalled carbon nanotube nanofibers were used as promising active layers for flexible nonvolatile data storage devices. Impressively, the chiral MoS_2 nanofiber-based memory device presents a typical nonvolatile flash memory effect with excellent reproducibility and good stability. Our method offers a general route for the preparation of various functional chiral nanostructures that might have wide applications.

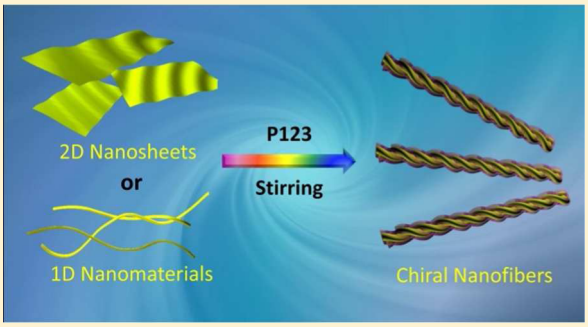

Chirality is widely expressed in nature, especially in biological molecules such as proteins and DNA, in which the helix is one of the most simple and important states.[1] Programming chirality into inorganic nanomaterials can potentially generate some unique properties that could be favorable for many novel applications, including chiral separation, chiral sensing, and enantioselective catalysis.[2−4] Self-assembly is a facile and feasible strategy that allows for the large-scale production of complex architectures with desired properties.[5−7] Especially, inorganic chiral nanostructures can be constructed via self-assembly of achiral components by using, for example, chiral templates,[8,9] light/tension/magnetism-induced self-assembly.[10−13] or the assistance of facet-selective polymers.[14] However, the aforementioned methods are only applicable for some specific materials and/or need chiral templates to direct the self-assembly.[8−14] To this end, providing a facile and general technique for engineering the chirality of various inorganic nanomaterials with various sizes, dimensionalities, compositions, and surface properties is highly desired but still remains a challenge.

Ultrathin low-dimensional nanomaterials, particularly two-dimensional (2D) nanosheets such as graphene and transition-metal dichalcogenides (TMDs),[15−17] one-dimensional (1D) nanomaterials such as multiwalled carbon nanotubes (MWCNTs) and metal/semiconducting nanowires,[18,19] and their functional composites[20,21] have been widely studied during the last few decades. The reduced dimensionality and ultrathin nature of these 2D and 1D nanomaterials endow them with many unconventional physical, chemical, and electronic properties, making them ideal candidates in a wide range of applications.[15−21] Of note, the fluidlike flexibility of these ultrathin nanomaterials enables their morphological/topological transformation via self-assembly. Herein we report a facile and universal method for the high-yield and scalable preparation of chiral nanofibers and nanorings from various 2D (e.g., graphene oxide (GO) and TMDs) and 1D nanomaterials (e.g., MWCNTs and AgAu nanowires) via a polymer-assisted self-assembly process in vigorously stirred solution. Impressively, the chiral-nanofiber-based composites can be used as active materials in flexible nonvolatile memory devices. As a proof-of-concept application, chiral MoS_2 and

Received: November 7, 2014
Published: January 12, 2015

DOI: 10.1021/ja511471b
J. Am. Chem. Soc. 2015, 137, 1565−1571

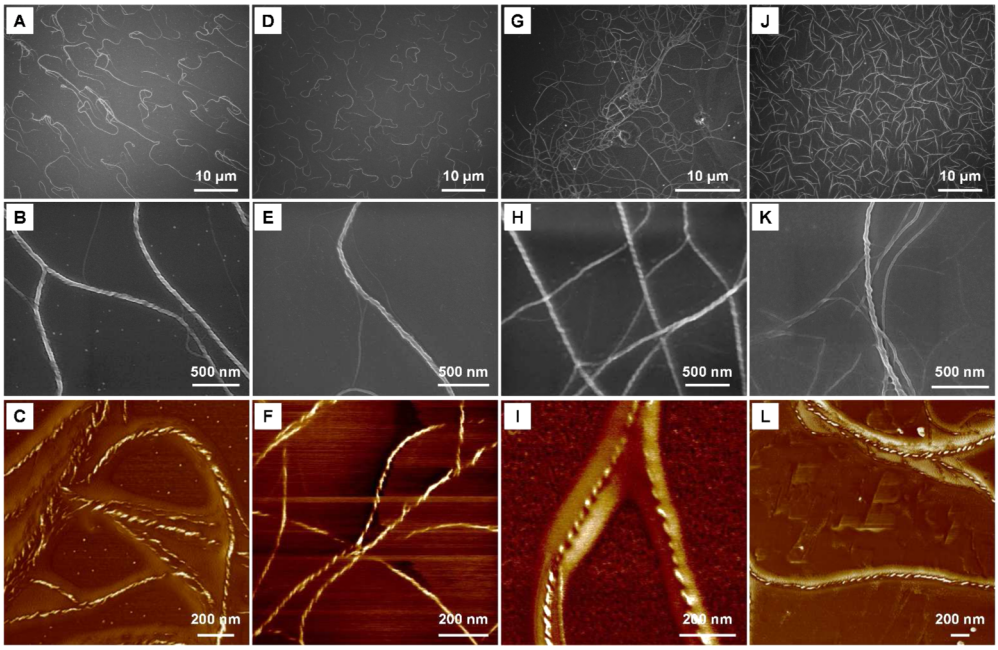

Figure 1. (A, B) SEM images and (C) AFM phase image of chiral GO nanofibers. (D, E) SEM images and (F) AFM phase image of chiral MoS_2 nanofibers. (G, H) SEM images and (I) AFM phase image of chiral TaS_2 nanofibers. (J, K) SEM image and (L) AFM phase image of chiral MWCNT nanofibers.

MWCNT nanofiber-based devices exhibit the flash and write-once-read-many-times (WORM) memory effect, respectively. Importantly, the former device shows excellent reproducibility and good stability.

In our experiments, several kinds of low-dimensional nanomaterials were chosen to demonstrate our proposed general strategy for the preparation of chiral nanofibers. Briefly, an aqueous solution containing ultrathin low-dimensional nanomaterials was added dropwise to a vigorously stirred polymer aqueous solution (see the Experimental Section for details). The polymer used here was Pluronic P123, an achiral triblock copolymer ($PEO_{20}PPO_{70}PEO_{20}$; its molecular structure is shown in Figure S1 in the Supporting Information). After the resultant products were washed, they were characterized by scanning electron microscopy (SEM) and atomic force microscopy (AFM). For example, GO nanofibers with lengths of 10−50 μm (Figure 1A) were prepared from single-layer GO nanosheets with sizes of up to 20 μm and a thickness of ∼0.9 nm (Figure S2). The yield of the produced chiral GO nanofibers was almost 100% (Figure 1A). The left-handed spiral structure of the GO nanofibers with diameters of 40 ± 12 nm can be clearly observed in SEM and AFM phase images (Figure 1B,C). The enantiomeric purity, i.e., 100% left-handed helix, was confirmed by randomly measuring more than 200 GO nanofibers by SEM. The section analysis of the AFM phase image indicated that the average pitch length of the GO nanofibers was ∼42 nm (Figure S3). The Raman spectrum of chiral GO nanofibers exhibited the same D (1345 cm^{-1}) and G (1595 cm^{-1}) bands shown in GO nanosheets (Figure S4), further confirming that the nanofibers were constructed from GO sheets. It should be noted that the diameters of the chiral GO nanofibers can be controlled by changing the initial concentration of GO nanosheets. For example, the diameters of GO nanofibers prepared at high (0.25 μg mL^{-1}), middle (0.1 μg mL^{-1}), and low (0.05 μg mL^{-1}) concentrations were 65 ± 18 nm (Figure S5A), 45 ± 10 nm (Figure S5B), and 27 ± 13 nm (Figure S5C), respectively.

Impressively, our method is general and can also be used to prepare chiral TMD nanofibers from TMD nanosheets. For example, SEM and AFM height images showed that the size and thickness of single-layer MoS_2 nanosheets used for the self-assembly process were 0.5−2 μm and ∼1.0 nm, respectively (Figure S6). The MoS_2 nanosheets could also be assembled into left-handed chiral nanofibers with lengths of 10−20 μm (Figure 1D), an average diameter of 30 ± 11 nm (Figure 1E,F), and a pitch length of ∼39 nm (Figure S7). Like the chiral GO nanofibers, the chiral MoS_2 nanofibers also showed 100% enantiomeric purity with left-handedness on the basis of an investigation of 200 randomly chosen nanofibers. The circular dichroism (CD) spectrum of MoS_2 nanofibers showed two broad bands at around 253 and 298 nm (Figure 2), indicating

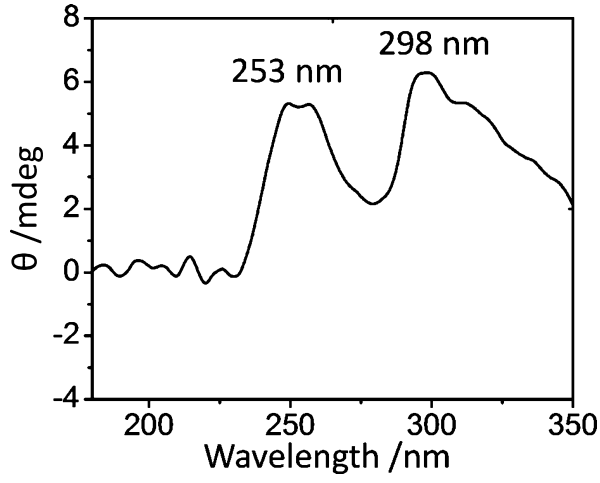

Figure 2. CD spectrum of chiral MoS_2 nanofibers at a concentration of 0.1 μg mL^{-1}.

DOI: 10.1021/ja511471b
J. Am. Chem. Soc. 2015, 137, 1565−1571

their chiral nature.[22] Raman characterization further confirmed that the nanofibers were constructed from MoS_2 nanosheets (Figure S8). Moreover, we also prepared other left-handed nanofibers (Figure 1G–I, Figure 3, and Figure S9) in high yield from single-layer TaS_2 (Figure S10A) and TiS_2 nanosheets (Figure S10B) as well as few-layer $TaSe_2$ (Figure S10C) and WSe_2 nanosheets (Figure S10D).

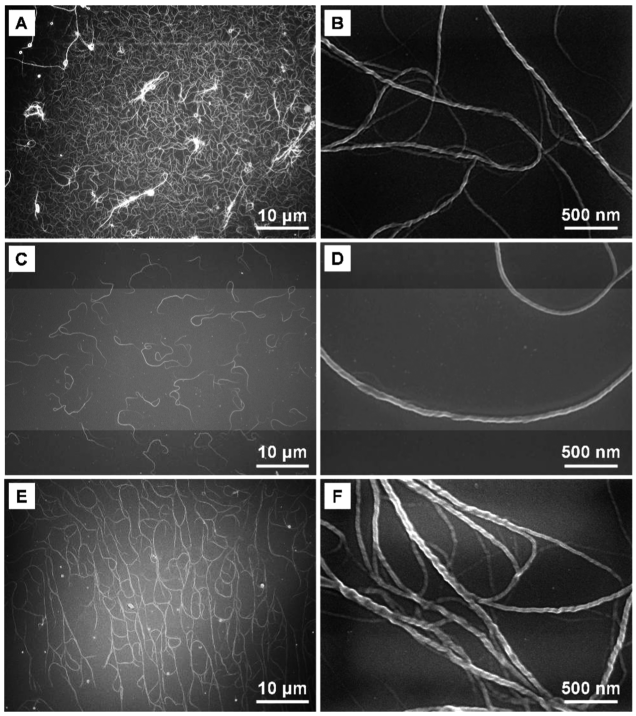

Figure 3. SEM images of chiral (A, B) TiS_2, (C, D) $TaSe_2$, and (E, F) WSe_2 nanofibers.

To further demonstrate the applicability of our method for complex systems, Pt-coated MoS_2 and reduced graphene oxide (rGO) composites, denoted as Pt-MoS_2 and Pt-rGO, respectively, were used to prepare hybrid chiral nanofibers. Transmission electron microscopy (TEM) images of Pt-MoS_2 and Pt-rGO are shown in Figure S11. After the polymer-assisted self-assembly, the Pt-MoS_2 or Pt-rGO hybrids were transformed into nanohelices with morphology and spiral structure (Figure S12) similar to those of chiral MoS_2 nanofibers (Figure 1D,E). It should be noted that both of the hybrid nanohelices were 100% left-handed chiral structures.

Besides 2D nanostructures, the self-assembly of 1D nanomaterials into chiral nanofibers can also be achieved through a similar strategy. Herein, MWCNTs and AuAg nanowires were used as examples. The lengths and diameter of the MWCNTs were 1–5 μm and 10 nm, respectively (Figure S13A,B), and those of AuAg nanowires were 1–5 μm and 2–3 nm, respectively (Figure S13C,D). As shown in Figure 1J, left-handed chiral MWCNT nanofibers with lengths of 20–50 μm and an average diameter of 20 ± 12 nm (Figure 1K,L) were obtained in high yield. The AFM phase image in Figure 1L further confirmed the formation of chiral MWCNT nanofibers with an average pitch length of ~80 nm (Figure S14). The chiral MWCNT nanofibers showed a Raman spectrum similar to that of the MWCNTs (Figure S15), proving that the helices were assembled from MWCNTs. Similar results were also obtained for the chiral AuAg nanofibers (Figure 4).

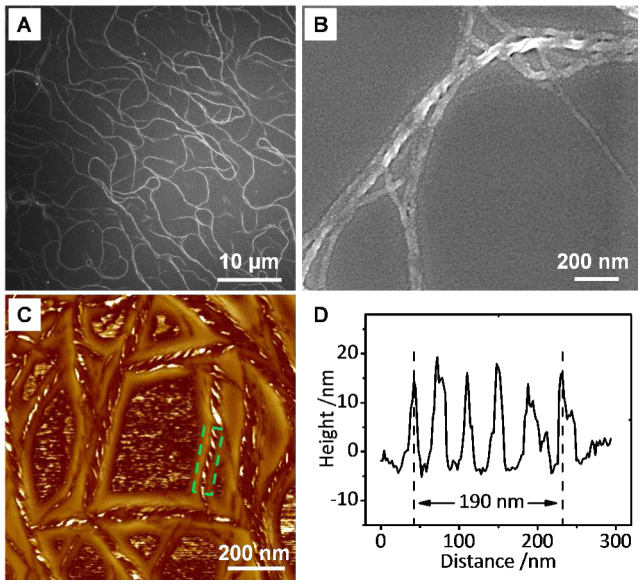

Figure 4. (A, B) SEM images, (C) AFM phase image, and (D) the corresponding section analysis of chiral AuAg nanofiber shown in the dashed rectangle in (C).

To study the mechanism of the self-assembly process, a series of control experiments were performed using MoS_2 as an example. We found that chiral MoS_2 nanofibers were obtained only when MoS_2 nanosheets were vigorously stirred (at 1500 rpm here) in a solution containing a polymer like P123. Without stirring or in the absence of polymer, MoS_2 nanosheets maintained their 2D morphology after precipitation via centrifugation (Figure S16A–D). Therefore, both stirring and the addition of polymer are crucial to the formation of chiral nanofibers. It should be noted that P123 is achiral and that pure P123 precipitates as microparticles from its stirred aqueous solution (Figure S16E,F). In this case, we first studied the effect of stirring on the formation of chiral nanofibers. Stirring can generate a vortex in solution, which has been regarded as a typical example of macroscopic chirality in nature.[23] It has been demonstrated that dynamic chiral signals can be detected from the stirring aqueous solution containing achiral organic molecules, proving the dynamic formation of chiral architectures in the vortex.[24] However, the chiral signals could not be detected once the stirring stopped, indicating that the chiral structures only can exist in the stirring solution.[24] In our experiments, using GO as an example, we also found that reversible CD signals were detected under stirring (Figure S17), indicating that the GO nanosheets were twisted under vortex to form dynamical chiral structures. However, the CD signal of GO disappeared when the stirring was stopped without the addition of polymer (Figure S17), proving that the twisted structures became untwined when the stirring was stopped. Similar CD signals were also observed for the mixture of GO and P123 under stirring (Figure S18A). Impressively, the mixture still showed a CD signal even after the stirring was stopped, indicating that chiral structures of the mixture can exist (Figure S18B). Besides P123, other two commonly used achiral polymers, i.e., Tween 20 (Figure S19A) and Triton 100-X (Figure S19B), were also used to prepare chiral nanofibers. A similar phenomenon of chiral MoS_2 nanofiber formation was found (Figure S20). On the basis of the aforementioned experiments, we believe that the 1D or 2D nanomaterials are twisted into chiral nanofibers in the vigorously stirred solution

DOI: 10.1021/ja511471b
J. Am. Chem. Soc. 2015, 137, 1565–1571

by the vortex, and the polymer such as P123 mixed with them can help to maintain the chiral nanostructures even when the stirring stops.

Recently, the synthesis and assembly of 1D ring or coil nanostructures have also attracted much attention because of their potential applications in nanodevices such as fictional nanorobots.[25,26] Self-coiling from 1D nanostructures is one of the most promising strategies for the large-scale preparation of ringlike nanostructures.[26] However, to the best of our knowledge, the preparation of chiral nanorings has not been reported to date. Here we demonstrate that the obtained chiral nanofibers can be transformed into chiral nanorings through a controlled reassembly process (see the Experimental Section for the details). SEM images of typical chiral GO, WSe_2, and MWCNT nanorings are shown in Figure 5. It can be observed

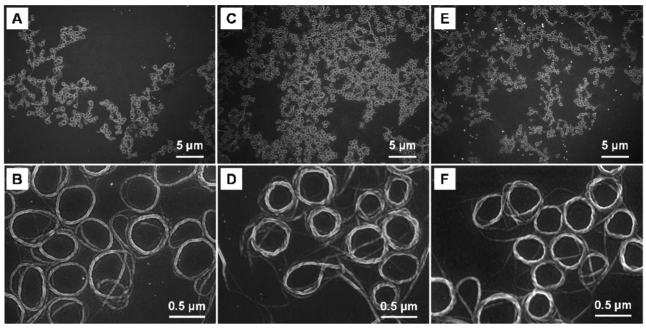

Figure 5. SEM images of chiral (A, B) GO, (C, D) WSe_2, and (E, F) MWCNT nanorings.

that chiral GO nanorings were prepared in high yield with ring diameters of ~400−600 nm (Figure 5A,B) from the chiral GO nanofibers (Figure 1B). In addition, the left-handedness of the nanofibers remained unchanged after their transformation into nanorings. Similarly, chiral nanorings of WSe_2 (Figure 5C,D), MWCNTs (Figure 5E,F), $TaSe_2$ (Figure S21A,B), and MoS_2 (Figure S21C,D) can also be prepared in high yield from the reassembly of their chiral nanofibers with the same left-handedness.

As is known, polymer-based nonvolatile memory devices are regarded as the most promising alternatives for traditional data storage devices because of their unique properties and advantages.[27] The hybridization of polymers with inorganic nanomaterials as active layers has been demonstrated to optimize their performance.[28,29] Compared with traditional electrodes, highly conductive, flexible, solution-processable, and transparent graphene films could be excellent electrode materials for future electronics.[30] Here, as a proof of concept, flexible memory devices with a configuration of rGO/active layer/rGO were fabricated by using rGO films as both the top and bottom electrodes and chiral MoS_2, MWCNT, or GO nanofibers containing P123 as the active layer. A photograph of fabricated flexible 6 × 6 devices based on chiral MoS_2 nanofibers is shown in Figure 6A. Each memory cell has a sandwich configuration in which the active layer is between two rGO electrodes (Figure 6A inset). The thickness of the active layer was about 100 nm, as confirmed by cross-sectional SEM analysis (Figure S22).

The memory performance of the fabricated devices was investigated. The current−voltage (I−V) characteristics of a chiral MoS_2 nanofiber-based device with the configuration rGO/MoS_2 nanofibers/rGO (Figure 6B−D) exhibit a typical

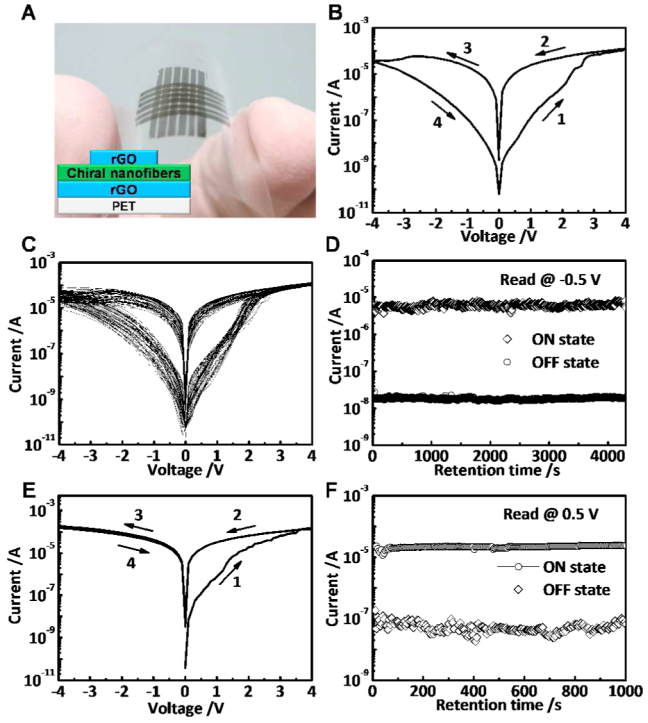

Figure 6. Memory devices based on chiral nanofibers. (A) Photograph of 6 × 6 flexible memory devices on PET. Inset: schematic illustration of the fabricated memory cell. (B) Initial I−V characteristics of a chiral MoS_2 nanofiber-based memory cell. (C) Consecutive I−V measurements on a chiral MoS_2 nanofiber-based memory cell. (D) Retention test of a chiral MoS_2 nanofiber-based memory device at a reading voltage of −0.5 V under ambient conditions. (E) Initial I−V characteristics of a chiral MWCNT nanofiber-based memory cell. (F) Retention test of a chiral MWCNT nanofiber-based memory device at a reading voltage of 0.5 V under ambient conditions.

flash memory effect. In Figure 6B, the current increased consecutively from ~5 × 10^{-11} to 10^{-4} A when a positively biased potential sweep from 0 to 4 V was applied (stage 1), where the device was set to the low-resistance state (LRS), i.e., the ON state. This process is defined as the "Write" process, which was supported by the subsequent backward sweep from 4 to 0 V (stage 2). The device remained in the LRS state in the following sweep from 0 to −4 V (stage 3). During the backward sweep from −4 to 0 V, the current decreased consecutively and returned to the initial OFF state (stage 4), which is defined as the "Erase" process. The whole process indicated that the chiral MoS_2 nanofiber-based device was a typical nonvolatile flash memory diode with an ON/OFF current ratio of 5.5 × 10^2. Furthermore, cyclic programming operations of the rGO/MoS_2 nanofibers/rGO memory cell were performed to investigate its stability. Impressively, even after more than 50 consecutive cycles, no obvious degradation was detected (Figure 6C), indicating the highly stable performance of our device. Figure 6D shows the retention property of the memory device at a read voltage of −0.5 V under ambient conditions. Its ON/OFF ratio showed only a slight change even after a test period of more than 4 × 10^3 s, indicating the excellent reliability of our device.

Besides the aforementioned device, a chiral MWCNT nanofiber-based diode was also fabricated by a similar process. The I−V characteristics of the chiral MWCNT nanofiber-based device showed a typical WORM memory effect (Figure 6E,F

DOI: 10.1021/ja511471b
J. Am. Chem. Soc. 2015, 137, 1565−1571

and Figure S23). As shown in Figure 6E, the resistance gradually decreased from the initial high-resistance state (HRS) when a positive voltage sweep from 0 to 4 V was applied (stage 1), during which the current increased from $\sim 3.5 \times 10^{-11}$ to 10^{-4} A. The resistive switching from the HRS (i.e., OFF state) to the LRS (i.e., ON state) is assignable to the "Write" process in the data storage operation. After that, the device remained in the ON state during the following sweeps (stages 2 and 3). Notably, the OFF state of this device could not be completely recovered by a reverse sweep (stage 4) and the second cycle (Figure S23), indicating that it is a typical nonvolatile WORM memory device with an ON/OFF current ratio of 10^2. However, the chiral GO nanofiber-based device showed a typical insulator characteristic and no memory effect (Figure S24). In addition, the device of two stacked rGO electrodes without any active layer showed good conductivity without a memory effect (Figure S25A), while an rGO/P123/rGO device showed a typical insulator behavior and no switching effect (Figure S25B). As is known, the pure MoS_2 nanosheets and MWCNTs are semiconducting and conducting materials, respectively, and generally exhibit no switching effect when they are used as active layers.[31,32] As mentioned above, both nonvolatile flash and WORM effects can be achieved in our memory devices by varying the active material. In this case, our chiral nanofibers might have great potential for flexible nonvolatile data storage applications.

The carrier transport mechanisms for the aforementioned two devices were investigated on the basis of the experimental and fitted data of their $I-V$ characteristics in the OFF and ON states (Figure 7). For the chiral MoS_2 nanofiber-based device,

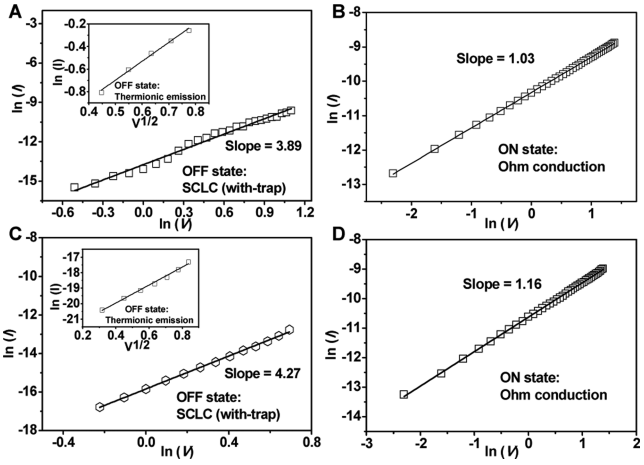

Figure 7. Experimental data and fitted lines for the $I-V$ characteristics of a chiral MoS_2 nanofiber-based device in the (A) OFF state and (B) ON state and a chiral MWCNT nanofiber-based device in the (C) OFF state and (D) ON state.

the experimental and fitted data for the $I-V$ characteristics were studied. In the OFF state, the plot of $\ln(I)$ versus $V^{1/2}$ from 0 to 0.8 V was fit to a straight line (Figure 7A inset), indicating that the conduction mechanism is probably thermionic emission.[38] The charge injection from the rGO electrode to the active layer dominated this process. After that, a linear relation with a slope of 4.27 was observed in the plot of $\ln(I)$ versus $\ln(V)$ for the voltage sweep from 0.9 to 2.5 V (Figure 7B), suggesting that the carrier transport process is dominated by the space-charge-limited current (SCLC) model.[39] The device showed Ohmic conduction behavior in the ON state (Figure 7B).[38] Moreover, because of the insulating property of the dielectric material (P123), the trapped charges in MoS_2 were retained after the power was turned off, enabling the high conductivity and nonvolatility of the memory device. It should be noted that the trapped charges were detrapped when a reverse bias was applied, indicating its flash type memory effect. The whole process is similar to the previously reported poly(vinylpyrrolidone)−MoS_2-based flash memory device.[40]

Similarly, the experimental and fitted data for the $I-V$ characteristics were investigated in order to study the carrier transport mechanism of the chiral MWCNT nanofiber-based device (Figure 7C,D). In the first three stages, the MWCNT-based device showed a carrier transport mechanism similar to that of the MoS_2-based device. However, unlike the chiral MoS_2 nanofiber-based device, the trapped charges could not be detrapped when a reverse bias was applied, indicating its WORM-type memory effect.[41] The highly conductive nature of MWCNTs could be the reason for its different switching behavior compared with the semiconductor MoS_2 when used as the active layer in memory devices, which is consistent with previously reported results.[40,41]

In summary, we have developed a facile and universal strategy for self-assembly of various ultrathin low-dimensional nanostructures to form chiral nanofibers and nanorings. Various materials with different compositions or dimensionalities, such as metals (e.g., AuAg nanowires), carbonaceous materials (e.g., MWCNTs and GO), and semiconductors (MoS_2, TiS_2, TaS_2, $TaSe_2$, and WSe_2), can be assembled into chiral nanofibers with 100% left-handedness. Same-handed chiral nanorings can be obtained from the chiral nanofibers via a reassembly process. Flexible nonvolatile memory devices based on the use of chiral nanofibers as active materials exhibited tunable switching behaviors. A highly reproducible rewritable flash effect and good stability were achieved with the chiral MoS_2 nanofiber-based device. We believe that our general strategy could be further extended to the assembly of other kinds of ultrathin 1D and 2D nanomaterials into chiral nanoarchitectures for various applications.

EXPERIMENTAL SECTION

Chemicals. Molybdenum disulfide (MoS_2, Rose Mill), titanium sulfide (TiS_2, Sigma), tantalum sulfide (TaS_2, Alfa Aesar), tantalum selenide ($TaSe_2$, Alfa Aesar), and tungsten selenide (WSe_2, Alfa Aesar) were used as received for the preparation of single-layer and few-layer 2D nanosheets by means of the electrochemical lithium interaction method recently developed by our group.[33] Natural graphite (purchased from BayCarbon, Bay City, MI, USA) was used to synthesize GO by a modified Hummers method.[34] The AuAg alloy nanowires were synthesized by means of the reported method.[35] Pt nanoparticles (NPs) were grown on the single-layer MoS_2 and rGO to form Pt NP-based composites (i.e., Pt-MoS_2 and Pt-rGO, respectively) by means of the reported photochemical reduction method.[36] Pluronic P123 (molecular weight (MW) 5800), Triton X-100 (MW 646.8), Tween 20 (MW 1227.5), flexible polyethylene terephthalate (PET) film, ethanol (absolute, 99.8%), tetrahydrofuran (THF, 99.8%), and MWCNTs were purchased from Sigma-Aldrich and used as received. Ultrapure Milli-Q water (Milli-Q System, Millipore, Billerica, MA, USA) was used in all of the experiments.

Preparation of Chiral Nanofibers. Ultrathin nanomaterials (e.g., GO) were dispersed in water with a certain concentration (e.g., [GO] = 0.1 μg mL^{-1}). P123 was dissolved in water at a concentration of 8 mg mL^{-1}. After 2 mL of GO suspension was added dropwise to 5 mL of P123 solution, the mixture was stirred at high speed (~1500 rpm) on a magnetic stirrer at room temperature. The mixed solution was further stirred for 20 min, and GO nanosheets self-assembled to give

DOI: 10.1021/ja511471b
J. Am. Chem. Soc. 2015, 137, 1565−1571

chiral nanofibers. The final product was washed twice with water and then once with THF. A drop of the chiral nanofiber suspension was placed on a Si or Si/SiO_2 wafer and naturally dried in air prior to further characterization. The other chiral nanofibers made from MoS_2, TiS_2, TaS_2, $TaSe_2$, WSe_2, Pt-MoS_2, Pt-rGO, MWCNTs, and AuAg nanowires were prepared by the same process as for the chiral GO nanofibers. The experiments using other polymers such as Triton X-100 and Tween 20 in place of P123 were performed under the same experimental conditions.

Assembly of Chiral Nanofibers into Nanorings. The chiral nanorings were prepared by a secondary self-assembly process. After the chiral nanofibers were obtained, 400 μL of the nanofiber solution was transferred into a 1.5 mL centrifuge tube and then washed with water through sonication for 1 min and vortexing for 5 min on a vortex mixer at low speed before centrifugation to remove the upper solution. This procedure was repeated once. After that, 980 μL of THF and 20 μL of ethanol were added consecutively to the centrifuge tube to form a suspension, which was then sonicated for 1 min and oscillated on a vortex mixer for about 30 min before centrifugation to remove the upper solution. Finally, 990 μL of THF and 10 μL of ethanol were added consecutively to the centrifuge tube, which was sonicated for 1 min and then oscillated on a vortex mixer for 5 min. After the resultant solution was centrifuged at 13 000 rpm for 2 min, the upper solution was removed, and the precipitate was collected. The obtained precipitate consisting of the formed chiral nanorings was dispersed in THF, and this solution was then dropped on Si or Si/SiO_2 wafer and naturally dried in air prior to further characterization.

Fabrication of Flexible Memory Devices. First, patterned rGO electrodes on PET, denoted as PET/rGO, were prepared as bottom electrodes by means of our previously published method.[37] To make each device, a nanofiber solution in THF with a concentration of ~2 $\mu g\ mL^{-1}$ was spin-coated on top of the rGO electrode at 500 rpm for 5 s, 1000 rpm for 30 s, and then 3000 rpm for 30 s. The PET/rGO electrode coated with the active material was then dried overnight at 60 °C under vacuum. After that, another patterned rGO electrode, perpendicularly aligned with the bottom rGO electrode, was transferred onto the surface of the active material.[37] Finally, the prepared device was dried overnight at 60 °C under vacuum prior to further characterization.

Characterizations. SEM images were taken on JEOL 7600F scanning electron microscope at an accelerating voltage of 5 kV. Tapping-mode AFM images were obtained on Dimension 3100 atomic force microscope with a Nanoscope IIIa controller (Veeco, Fremont, CA, USA) under ambient conditions. CD measurements were conducted on Jasco J-810 spectropolarimeter (using a quartz cuvette with an optical length of 10 mm). Raman spectra were measured at room temperature using a WITec CRM200 confocal Raman microscopy system with the 488 nm excitation line and an air-cooled charge-coupled device as the detector (WITec Instruments, Ulm, Germany). The Raman band of a silicon wafer at 520 cm^{-1} was used as the reference to calibrate the spectrometer. TEM images were taken on JEOL JEM-2100F transmission electron microscope at an accelerating voltage of 200 kV. Optical microscopy images were taken on a Nikon Eclipse LV100 optical microscope. A Keithley 4200 semiconductor parameter analyzer was used to measure the $I-V$ characteristics of memory devices under ambient conditions.

■ ASSOCIATED CONTENT

Ⓢ Supporting Information

SEM images, TEM images, AFM images, CD spectra, Raman spectra, and molecular structures. This material is available free of charge via the Internet at http://pubs.acs.org.

■ AUTHOR INFORMATION

Corresponding Author

*hzhang@ntu.edu.sg

Notes

The authors declare no competing financial interest.

■ ACKNOWLEDGMENTS

This work was supported by MOE under AcRF Tier 2 (ARC 26/13, MOE2013-T2-1-034), AcRF Tier 1 (RG 61/12, RGT18/13, and RG5/13), Start-Up Grant (M4080865.070.706022), Singapore Millennium Foundation, and the National Research Foundation in Singapore. This research was also conducted by the NTU−HUJ−BGU Nanomaterials for Energy and Water Management Programme under the Campus for Research Excellence and Technological Enterprise (CREATE), which is supported by the National Research Foundation, Prime Minister's Office, Singapore. L.H.X. acknowledges the financial support from the National Natural Science Funds for Excellent Young Scholar of China (Grant No. 21322402).

■ REFERENCES

(1) Youatt, J. B.; Brown, R. D. *Science* **1981**, *212*, 1145.
(2) Wang, Y.; Xu, J.; Wang, Y. W.; Chen, H. Y. *Chem. Soc. Rev.* **2013**, *42*, 2930.
(3) Gao, P. X.; Ding, Y.; Mai, W. J.; Hughes, W. L.; Lao, C. S.; Wang, Z. L. *Science* **2005**, *309*, 1700.
(4) Che, S. A.; Liu, Z.; Ohsuna, T.; Sakamoto, K.; Terasaki, O.; Tatsumi, T. *Nature* **2004**, *429*, 281.
(5) Whitesides, G. M.; Grzybowski, B. *Science* **2002**, *395*, 2418.
(6) Park, S.; Lim, J. H.; Chung, S. W.; Mirkin, C. A. *Science* **2004**, *303*, 348.
(7) Mann, S. *Nat. Mater.* **2009**, *8*, 781.
(8) Sharma, J.; Chhabra, R.; Cheng, A. C.; Brownell, J.; Liu, Y.; Yan, H. *Science* **2009**, *323*, 112.
(9) Kuzyk, A.; Schreiber, R.; Fan, Z. Y.; Pardatscher, G.; Roller, E.-M.; Högele, A.; Simmel, F. C.; Govorov, A. O.; Liedl, T. *Nature* **2012**, *483*, 311.
(10) Srivastava, S.; Santos, A.; Critchley, K.; Kim, K.-S.; Podsiadlo, P.; Sun, K.; Lee, J.; Xu, C.; Lilly, G. D.; Glotzer, S. C.; Kotov, N. A. *Science* **2010**, *327*, 1355.
(11) Yeom, J.; Yeom, B.; Chan, H.; Smith, K. W.; Dominguez-Medina, S.; Bahng, J. H.; Zhao, G.; Chang, W. S.; Chang, S. J.; Chuvilin, A.; Melnikau, D.; Rogach, A. L.; Zhang, P.; Link, S.; Král, P.; Kotov, N. A. *Nat. Mater.* **2014**, *14*, 66.
(12) Gibaud, T.; Barry, E.; Zakhary, M. J.; Henglin, M.; Ward, A.; Yang, Y.; Berciu, C.; Oldenbourg, R.; Hagan, M. F.; Nicastro, D.; Meyer, R. B.; Dogic, Z. *Nature* **2012**, *481*, 348.
(13) Singh, G.; Chan, H.; Baskin, A.; Gelman, E.; Repnin, N.; Král, P.; Klajn, R. *Science* **2014**, *345*, 1149.
(14) Yu, S. H.; Cölfen, H.; Tauer, K.; Antonietti, M. *Nat. Mater.* **2005**, *4*, 51.
(15) Geim, A. K.; Novoselov, K. S. *Nat. Mater.* **2007**, *6*, 183.
(16) Nicolosi, V.; Chhowalla, M.; Kanatzidis, M. G.; Strano, M. S.; Coleman, J. N. *Science* **2013**, *340*, No. 1226419.
(17) Chhowalla, M.; Shin, H. S.; Eda, G.; Li, L. J.; Loh, K.; Zhang, H. *Nat. Chem.* **2013**, *5*, 263.
(18) de Jonge, N.; Lamy, Y.; Schoots, K.; Oosterkamp, T. H. *Nature* **2002**, *420*, 393.
(19) Xia, Y.; Yang, P.; Sun, Y.; Wu, Y.; Mayers, B.; Gates, B.; Yin, Y.; Kim, F.; Yan, H. *Adv. Mater.* **2003**, *15*, 353.
(20) Huang, X.; Qi, X. Y.; Boey, F.; Zhang, H. *Chem. Soc. Rev.* **2012**, *41*, 666.
(21) Tan, C. L.; Zhang, H. *Chem. Soc. Rev.* **2015**, DOI: 10.1039/c4cs00182f.
(22) Keller, D.; Bustamante, C. *J. Chem. Phys.* **1986**, *84*, 2972.
(23) Hama, F. R.; Nutant, J. *Phys. Fluids* **1961**, *4*, 28.
(24) Tsuda, A.; Alam, M. A.; Harada, T.; Yamaguchi, T.; Ishii, N.; Aida, T. *Angew. Chem., Int. Ed.* **2007**, *46*, 8198.
(25) Kong, X. Y.; Ding, Y.; Yang, R. S.; Wang, Z. L. *Science* **2004**, *303*, 1348.
(26) Chen, L. Y.; Wang, H.; Xu, J.; Shen, X. S.; Yao, L.; Zhu, L. F.; Zeng, Z. Y.; Zhang, H.; Chen, H. Y. *J. Am. Chem. Soc.* **2011**, *133*, 9654.

DOI: 10.1021/ja511471b
J. Am. Chem. Soc. 2015, 137, 1565−1571

(27) Lin, W. P.; Liu, S. J.; Gong, T.; Zhao, Q.; Huang, W. *Adv. Mater.* **2014**, *26*, 570.
(28) Tseng, R. J.; Tsai, C. L.; Ma, L. P.; Ouyang, J. Y.; Ozkan, C. S.; Yang, Y. *Nat. Nanotechnol.* **2006**, *1*, 72.
(29) Lee, J. S.; Cho, J.; Lee, C.; Kim, I.; Park, J.; Kim, Y.-M.; Shin, H.; Lee, J.; Caruso, F. *Nat. Nanotechnol.* **2007**, *2*, 790.
(30) Eda, G.; Fanchini, G.; Chhowalla, M. *Nat. Nanotechnol.* **2008**, *3*, 270.
(31) Yin, Z. Y.; Zeng, Z. Y.; Liu, J. Q.; He, Q. Y.; Chen, P.; Zhang, H. *Small* **2013**, *9*, 727.
(32) Sun, G. Z.; Liu, J. Q.; Zheng, L. X.; Huang, W.; Zhang, H. *Angew. Chem., Int. Ed.* **2013**, *52*, 13351.
(33) Zeng, Z. Y.; Yin, Z. Y.; Huang, X.; Li, H.; He, Q. Y.; Lu, G.; Boey, F.; Zhang, H. *Angew. Chem., Int. Ed.* **2011**, *50*, 11093.
(34) Hummers, W. S.; Offeman, R. E. *J. Am. Chem. Soc.* **1958**, *80*, 1339.
(35) Wang, Y.; Wang, Q.; Sun, H.; Zhang, W.; Chen, G.; Wang, Y.; Shen, X.; Han, Y.; Lu, X.; Chen, H. *J. Am. Chem. Soc.* **2011**, *133*, 20060.
(36) Huang, X.; Zeng, Z. Y.; Bao, S. Y.; Wang, M. F.; Qi, X. Y.; Fan, Z. X.; Zhang, H. *Nat. Commun.* **2013**, *4*, No. 1444.
(37) Liu, J. Q.; Yin, Z. Y.; Cao, X. H.; Zhao, F.; Wang, L. H.; Huang, W.; Zhang, H. *Adv. Mater.* **2013**, *25*, 233.
(38) Sze, S. M. *Physics of Semiconductor Devices*; Wiley: New York, 1981.
(39) Lampert, M. A.; Mark, P. *Current Injection in Solids*; Academic Press: New York, 1970.
(40) Liu, J. Q.; Zeng, Z. Y.; Cao, X. H.; Lu, G.; Wang, L. H.; Fan, Q. L.; Huang, W.; Zhang, H. *Small* **2012**, *8*, 3517.
(41) Liu, G.; Ling, Q.-D.; Kang, E.-T.; Neoh, K.-G.; Liaw, D.-J.; Chang, F.-C.; Zhu, C.-X.; Chan, D. S.-H. *J. Appl. Phys.* **2007**, *102*, No. 024502.

DOI: 10.1021/ja511471b
J. Am. Chem. Soc. 2015, 137, 1565−1571